Nuclear Engineering and Technology 53 (2021) 2261–2267

Contents lists available at ScienceDirect

Nuclear Engineering and Technology

journal homepage: www.elsevier.com/locate/net

Original Article

Magnesium potassium phosphate cements to immobilize radioactive concrete wastes generated by decommissioning of nuclear power plants

Jae-Young Pyo, Wooyong Um, Jong Heo*

Division of Advanced Nuclear Engineering, Pohang University of Science and Technology (POSTECH), Pohang, Gyeongbuk, 37673, Republic of Korea

ARTICLE INFO

Article history:
Received 6 September 2020
Received in revised form
21 December 2020
Accepted 5 January 2021
Available online 12 January 2021

Keywords:
Magnesium potassium phosphate cements (MKPCs)
Waste immobilization
Radioactive concrete wastes
Waste acceptance criteria
Leachability index

ABSTRACT

This paper evaluates the efficacy of magnesium potassium phosphate cements (MKPCs) as waste forms for the solidification of radioactive concrete powder wastes produced by the decommissioning of nuclear power plants. MKPC specimens that contained up to 50 wt% of simulated concrete powder wastes (SCPWs) were evaluated. We measured the porosity and compressive strength of the MKPC specimens, observing them using scanning electron microscopy and X-ray diffraction. The addition of SCPWs reduced the porosity and increased the compressive strength of the MKPC specimens. Struvite-K crystals were well-synthesized, and no additional crystal phase was formed. After thermal cycling and after immersion, MKPC specimens with 50 wt% SCPWs satisfied the waste-acceptance criteria (WAC) for compressive strength. Semi-dynamic leaching tests were performed using the ANS 16.1 method; the leachability indices of Cs, Co, and Sr were 11.45, 17.63, and 15.66, respectively, which also satisfy the WAC. Thus, MKPCs can provide stable matrices to immobilize radioactive concrete wastes generated by the decommissioning of nuclear power plants.

1. Introduction

Managing the waste that results from dismantling nuclear facilities is a serious challenge. By the end of 2018, approximately 170 nuclear power reactors had been permanently shut down, including Kori unit 1 in South Korea in 2017 [1]. The dismantling of gas-cooled and pressurized water reactors is expected to generate 750 and 900 tonnes of radioactive concrete waste, respectively [2]. Activation and contamination events are the primary sources of radioactive concretes in nuclear power plants. Activated concretes are generated when radionuclides accumulate in the concretes surrounding the reactor during operation [3]. Due to their large neutron-capture cross-sections, ^{60}Co, ^{152}Eu, and ^{154}Eu are responsible for most of the total accumulated radioactivity [4]. The radioactivity of the concretes adjacent to the reactor is high at the surface and gradually decreases with depth. Contaminated concretes are generated through exposure to radioactive liquids and aerosols during operation and decommissioning processes [3]. The typical radionuclides in contaminated concretes are ^{137}Cs, ^{90}Sr, and ^{60}Co, along with several fission products [5]. The adsorption of Cs on the mineral phases of concrete is well documented [6].

Contaminated concrete surfaces can be mechanically or chemically separated from the bulk. Mechanical methods include scabbling, shaving, and abrasive blasting [3,7,8]. Chemical decontamination techniques employ various acids, chelating agents, and electro-kinetic methods, with the advantages of being nondestructive and producing minimal secondary products [9–11]. However, it is difficult to achieve a clearance level when removing deeply-penetrated radionuclides using chemical approaches [12], so heating and grinding processes are used to decontaminate such concretes. During the dismantling of the Korea research reactor-2 (KRR-2), 260 tonnes of radioactive concrete were generated [13]. Most of the radionuclides were adsorbed on the porous cement pastes, not on aggregates [11], so the volume could be reduced by removing the aggregates. This process involves heating at 300–700 °C, pulverization, then sieving to obtain cement paste powders with particles of <1 mm diameter, which contains most of the ^{60}Co nuclide. The aggregates with diameters >1 mm can be treated as exempt wastes, reducing the waste volume by > 80% [13]. The remaining radioactive cement powders must be immobilized for disposal using solidification processes.

* Corresponding author.
E-mail address: jheo@postech.ac.kr (J. Heo).

https://doi.org/10.1016/j.net.2021.01.005

The objective of this work was to evaluate the potential of magnesium potassium phosphate cements (MKPCs) to solidify cement paste powders generated from heating and grinding radioactive concrete wastes. MKPCs consist of the struvite-K ($MgKPO_4 \cdot 6H_2O$) phase formed by the acid-base reaction of calcined magnesia and potassium dihydrogen phosphate in aqueous solution according to Eq (1) [14]:

$$MgO + KH_2PO_4 + 5H_2O = MgKPO_4 \cdot 6H_2O. \quad (1)$$

The advantages of MKPCs include high early strength, high bonding strength, little drying shrinkage, low permeability, and high sulfate resistance [15–17]. Several studies have been investigated the use of MKPCs for the solidification and stabilization of radioactive or heavy metal wastes [18–20]. The compressive strengths of MKPC waste forms are approximately two times higher than those of the ordinary Portland cement grouts, and the porosities are reduced by half [21]. In addition, MKPCs exhibit higher resistance against radioactivity compared to Portland cement [22,23], confirming the potential of MKPCs for radioactive waste solidification. In addition, unlike vitrification or ceramic solidification processes, MKPCs are cost- and energy-efficient and use simple equipment, especially there is no volatilization of nuclides. In this study, we added up to 50 wt% cement paste powder waste to MKPCs. The effect of the waste on MKPC microstructure was investigated using mercury intrusion porosimetry (MIP), scanning electron microscopy (SEM), and X-ray diffraction (XRD) methods. We also determined whether MKPC monoliths meet the waste-acceptance criteria (WAC) for disposal in repositories [24].

2. Materials and methods

2.1. Preparation of simulated concrete powder wastes (SCPWs)

Simulated concretes were prepared according to the concrete composition (Table 1) used in the construction of nuclear power plants in South Korea [25]. The concretes were composed of type-I Portland cement (Ssangyong Cement Industrial Co., Ltd., Korea), class-F fly ash, standard sand (ISO 679), coarse aggregates (4–16 mm), and a water-reducing agent (polycarboxylate ether superplasticizer). The chemical composition of type-I Portland cement and class-F fly ash (Table 2) were determined using X-ray fluorescence (XRF). Cylindrical concrete specimens (10 cm diameter, 20 cm height) were cast and cured at room temperature (20–25 °C) and relative humidity (RH) > 80% for 30 d. The concrete specimens were then heated at 550 °C for 1 h, crushed, and sieved through 1-mm mesh. The resulting powders were pulverized with a ball mill for 1 h to prepare simulated concrete powder wastes (SCPWs). These SCPWs were classified into size classes of <75 μm, 75–150 μm, 150–500 μm, and >500 μm. The chemical composition of each group was analyzed using XRF. Finally, the SCPW particle-size distribution was quantified using a laser particle-size analyzer (Mastersizer2000, Marvin, UK).

Table 1
Relative proportions of the simulated concrete ingredients.

Ingredient	wt%
Water	7.20
Cement	14.40
Fly ash	3.60
Sand	33.14
Gravel	41.54
Superplasticizer	0.12
Total	100.00

Table 2
Chemical compositions of fly ash, type I Portland cement, and calcined magnesia analyzed using X-ray fluorescence [wt%].

Compound	Source		
	Fly ash	Cement	Magnesia
SiO_2	61.17	19.9	4.16
Al_2O_3	20.1	4.9	0.9
Fe_2O_3	8.25	3.51	1.46
CaO	3.6	63.36	2.86
MgO	1.25	2.16	89.33
K_2O	1.25	1.06	–
TiO_2	0.86	0.27	–
Na_2O	0.85	0.17	–
SO_3	0.25	2.41	–
LOI	2.42	2.26	1.29
Total	100	100	100

2.2. Preparation of magnesium potassium phosphate cements (MKPCs)

MKPCs were synthesized from magnesia and potassium dihydrogen phosphate (KH_2PO_4) as shown in Eq (1) [14]. Dead burnt magnesia (DBM) was prepared by calcining MgO at > 1400 °C (Refractory Engineering Company Co., Ltd., Korea) [16]. DBM powder particle-size distribution was analyzed using the laser particle-size analyzer; the volumetric diameters were D_{10} = 7.32 μm, D_{50} = 24.9 μm, and D_{90} = 56.9 μm (Fig. 1). The concentration of MgO in the DBM powder was 89%, as determined using XRF (Table 2). Boric acid (H_3BO_3; Samchun, 99.5% purity) was used as a retarder to control the MKPC reaction rate [14]. Non-radioactive $Co(NO_3)_2 \cdot 6H_2O$ (Sigma-Aldrich, > 98% purity), $CsNO_3$ (Wako, > 99% purity), and $Sr(NO_3)_2$ (Alfa Aesar, > 99% purity) were used as surrogates for ^{60}Co, ^{137}Cs, and ^{90}Sr, respectively.

The optimal formulation of MKPC depends on its intended application [26]. The stoichiometric molar ratio of MgO (M):KH_2PO_4 (P):H_2O (W) for the synthesis of struvite-K is 1:1:5; however, several modifications have been attempted. MKPCs with a stoichiometric molar ratio prepared to solidify the liquid secondary wastes at a Hanford (USA) site resulted in the expansion of MKPC [27]. Additionally, MKPC swelling occurred when the molar ratio of

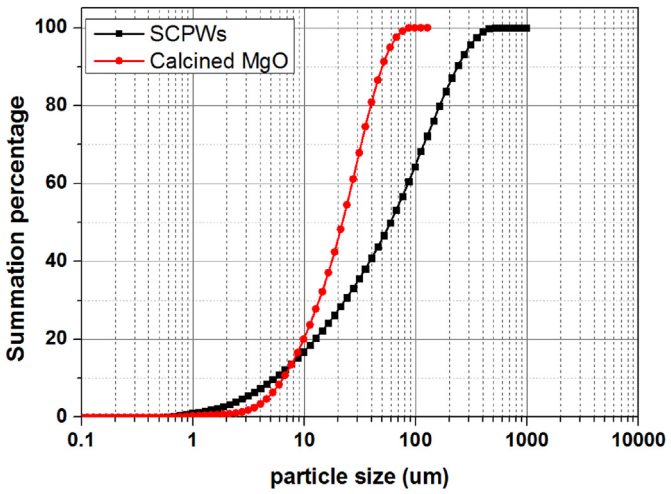

Fig. 1. Cumulative particle-size distributions in simulated concrete powder wastes (SCPWs) and calcined magnesia.

MgO and KH_2PO_4 (M/P) was fixed to one. The swelling diminishes as the M/P ratio increases [28]; however, the addition of excess MgO also accelerates the MKPC reaction rate, limiting the amount of waste loading [26]. Therefore, we fixed the M/P ratio to 1.5 to minimize MKPC swelling and maintain the appropriate reaction rate. When the molar ratio (W/P) of H_2O and KH_2PO_4 was <5, a portion of the KH_2PO_4 remained unreacted [29]. Residual KH_2PO_4 will degrade the water-resistance of MKPCs because KH_2PO_4 is highly soluble in water [30]. Therefore, we also fixed the W/P ratio to 5 to minimize the amount of unreacted KH_2PO_4.

2.3. SCPW and MKPC mixtures

SCPWs less than 1 mm in size generated by the heating and grinding processes were added to MKPC at 0 wt% (specimen W0), 25 wt% (W25), or 50 wt% (W50) (Table 3); 0.5 wt% of boric acid (H_3BO_3, Sigma-Aldrich) was added as a retarder [14]. No more than 50 wt% SCPWs could be added to MKPCs because of the difficulty of mixing the ingredient powders with a low water-to-solid ratio. $CsNO_3$, $Co(NO_3)_2{\cdot}6H_2O$, and $Sr(NO_3)_2$ powders (0.2 mol each) were mixed in deionized water (DIW).

It is preferable to add contaminants such as Cs, Co, and Sr ions directly to the SCPWs. Unfortunately, it was difficult to maintain a homogeneous distribution of Cs, Co, and Sr ion concentrations in the SCPWs; thus, we added them in the form of nitrates during MKPC synthesis. The MKPC raw materials and SCPWs were initially mixed at 200 rpm for 1 min using an overhead stirrer. DIW containing Cs, Co, and Sr nitrates was then added and mixed at 500 rpm for 10 min. The mixed pastes were cast into a polymethyl methacrylate mold to form 2 × 2 × 4 cm rectangular prisms. MKPC monoliths were removed from the mold after 24 h and cured at room temperature for 7, 14, or 28 d at RH > 80%.

2.4. Characterization

The compressive strength of cured specimens W0, W25, and W50 were measured using a universal testing machine at a loading rate of 0.25 MPa/s. The pore-size distribution in specimens that had been cured for 28 d was measured by mercury intrusion porosimetry (MIP) using a porosimeter (Autopore IV 9500, Micromeritics, USA). X-ray diffraction (XRD) patterns were recorded at $10^\circ \le 2\theta \le 50^\circ$ using a diffractometer (D/max-2500/PC, Rigaku, Japan) with Cu-Kα radiation at 40 kV tube voltage and 100 mA current. The morphology and chemical composition of the polished specimens were examined using an energy-dispersive X-ray spectroscope (EDS, Aztec EDS, Oxford Instruments, UK) attached to a scanning electron microscope (SEM, JSM-7100F, JEOL, Japan) at an accelerating voltage of 15 kV and a working distance of 10 mm.

We compared the characteristics of W50 specimens to the WAC after thermal-cycling and water-immersion tests. The thermal-cycling tests were conducted according to ASTM B 553–71 procedures for specimens that were cured for 28 d [31]. The specimens were exposed to 30 thermal cycles of heating to 60 °C and freezing to −40 °C. The heating and cooling rates were ±10 °C/h, and the specimens were held at the target temperature of 60 °C or −40 °C for 1 h each time. After the thermal cycles, we visually examined the surfaces of the specimens for cracks before measuring the compressive strength. Water immersion tests were performed following ANS 16.1 procedures to quantify the degradation of mechanical strength and the leaching characteristics of the specimens [32]. The compressive strength of the bulk specimens and the leached element concentrations in the water were analyzed after 90 d of immersion. The leachant was DIW with a conductivity <1 μS/cm. Specimens were immersed in DIW with a ratio of leachant volume [cm^3] to specimen surface area [cm^2] of 10 cm; the leaching agent was collected and replaced with fresh DIW after 2, 7, 24, 48, 72, 96, 120, 456, 1128, and 2160 h. The ion concentrations in the collected leachates were analyzed using inductively-coupled plasma mass spectrometry (ICP-MS, NexION 2000, PerkinElmer, USA) at RF power of 1600 W. The effective diffusivity D [cm^2/s] of each element was derived as

$$D = \pi \left[\frac{(a_n/A_0)}{(\Delta t)_n}\right]^2 \left(\frac{V}{S}\right)^2 T \quad (2)$$

where a_n [g] is the amount of an element released from the specimen during the specific leaching interval n; A_0 [g] is the initial concentration in the specimen; $(\Delta t)_n$ [s] is the leaching interval; V [cm^3] is the volume of the specimen; S [cm^2] is the geometric surface area of the specimen; and $T = \left[\frac{1}{2}(\sqrt{t_n} + \sqrt{t_{n-1}})\right]^2$, where t_n [s] is the time to the nth leaching interval. The leachability index (LI) is the sum of the negatives of the natural logarithms of the effective diffusivities:

$$\mathrm{LI} = \frac{1}{m}\sum_{n=1}^{m} [-\log(D)]_n \quad (3)$$

where n is the number of measurements and m is the total number of leaching periods.

Table 3
Formation [wt%] of magnesium potassium phosphate cement specimens containing 0 (W0), 25 (W25), and 50 wt% (W50) simulated concrete powder wastes (SCPWs).

Component	Specimen		
	W0	W25	W50
SCPW	0	25.00	50.00
MgO	20.24	15.15	10.07
KH_2PO_4	45.55	34.11	22.66
H_2O	29.50	22.09	14.68
H_3BO_3	0.50	0.50	0.50
$CsNO_3$	1.18	0.88	0.58
$Co(NO_3)_2{\cdot}6H_2O$	1.76	1.31	0.87
$Sr(NO_3)_2$	1.28	0.96	0.63
Total	100.00	100.00	100.00

3. Results and discussion

3.1. Simulated concrete powder wastes

The X-ray diffraction patterns (Fig. 2a) of SCPWs before heating show peaks from portlandite ($Ca(OH)_2$), quartz (SiO_2), K-feldspar ($KAlSi_3O_8$), plagioclase ($NaAlSi_3O_8$–$CaAl_2Si_2O_8$), and calcite ($CaCO_3$), as observed in previous studies [33,34]. Portlandites appear to form during the hydration of Portland cement. Quartz, K-feldspar, and plagioclase are present in the sand and crushed gravel. Calcium silicate hydrates (C–S–H) were not identified in hydrated Portland cement pastes due to their amorphous nature [35]. The portlandite peaks disappeared after heating because the cement was dehydrated at 450 °C [36]. After the heating process, SiO_2 and CaO are the main components of the final SCPWs (Table 4).

The particle size and composition of additives have a significant influence on the reaction of cementitious materials [37,38]. Therefore, we analyzed the composition of SCPWs with different particle sizes (Table 4). Particles with smaller diameters contained high concentrations of CaO, which was likely due to the difference in hardness between the cement pastes and aggregates. Cement pastes are softer than aggregates [39], resulting in fine particles

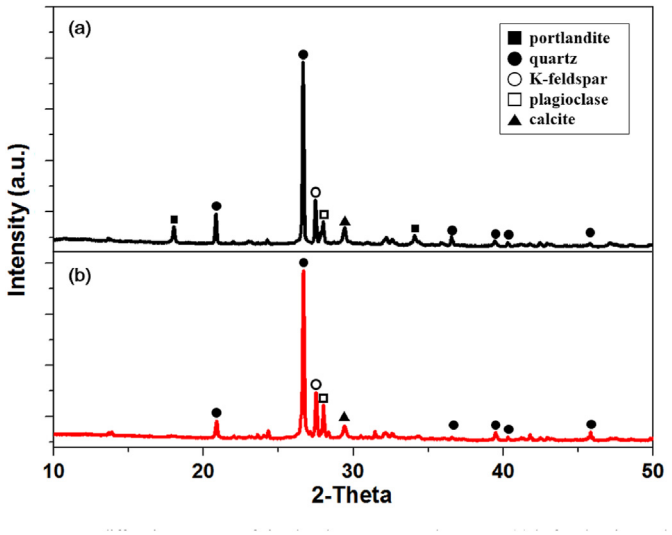

Fig. 2. X-ray diffraction patterns of simulated concrete powder wastes (a) before heating and (b) after heating.

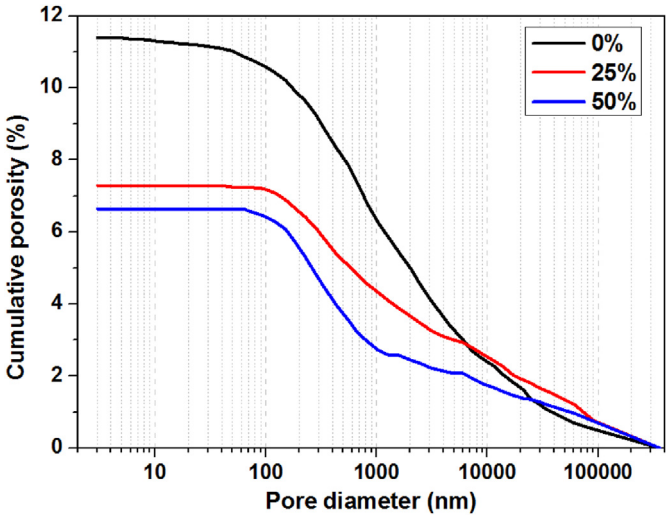

Fig. 3. Cumulative porosities of magnesium potassium phosphate cements containing 0, 25, or 50 wt% simulated concrete powder wastes.

Table 4
Compositions [wt%] of simulated concrete powder waste powders classified by diameter intervals. (Oxides of less than 1 wt% are not included.).

Compound	SCPW	Particle size [μm]			
		<75	75–150	150–500	>500
SiO_2	66.41	49.57	78.83	87.44	93.27
CaO	21.39	31.64	8.97	3.63	1.41
Al_2O_3	7.44	8.65	6.84	5.08	1.64
Fe_2O_3	2.65	3.39	1.51	1.41	1.21
Total	97.89	93.25	96.15	97.56	97.53

with diameters < 75 μm in the SCPWs; these fine powders are the target for solidification in the present study. Furthermore, these fine particles have large specific surface areas that bear radioactive ions [13], which are to be immobilized into MKPCs.

3.2. Compressive strength and pore structure of MKPCs

The MKPC compressive strength increased as the curing time and waste loading increased. The compressive strength of specimens cured for 28 d was 41.44 MPa, 55.64 MPa, and 56.27 MPa for W0, W25, and W50, respectively (Table 5). The W/P molar ratio was fixed at 5 in the starting mixture to satisfy the stoichiometry of struvite-K; the water-to-solid mass ratio decreased from 0.455 in W0 to 0.184 in W50. This result is consistent with previous reports that the compressive strength of MKPC increases as the water-to-solid ratio decreases with decreased porosity [40–42].

The specimen porosity ranged from 6 to 12% and decreased with the addition of SCPWs (Fig. 3). Cement-based materials contain three types of pores: air voids, capillary pores, and gel pores [43]. Air voids with characteristic dimensions of several micrometers are formed by entrainment of air during cement mixing. Capillary pores (50 nm–10 μm) are spaces between hydration products [44]. Gel pores (0.5–10 nm) exist inside hydration products [45]. Pores can also form in MKPCs as a consequence of volume reduction during the formation of struvite-K [46]. The molar volume of struvite-K is 143.03 cm^3/mol and the sum of the molar volumes of starting materials is 159.56 cm^3/mol; therefore, the formation of the struvite-K phase resulted in a volume reduction of approximately 10%, which contributed to the generation of pores in MKPCs. The MKPC pores were mainly capillary pores (Fig. 3), which are known to decrease as the water-to-cement ratio decreases [47], i.e., SCPWs act as inert fillers, so the addition of SCPWs decreased the porosity by decreasing the relative amounts of the components that lead to pore formation. We believe that the increase in compressive strength of the final MKPC specimens can also be attributed to the decreased porosity that resulted from SCPW addition.

Table 5
Mean ± standard deviation (n = 3) compressive strengths (MPa) of magnesium potassium phosphate cement specimens with simulated concrete powder waste contents of 0 (W0), 25 (W25), and 50 wt% (W50).

Curing period (d)	W0	W25	W50
7	34.52 ± 2.33	48.94 ± 2.33	45.75 ± 4.44
14	38.49 ± 3.29	51.94 ± 3.26	50.80 ± 2.12
28	41.44 ± 3.39	55.64 ± 9.26	56.27 ± 4.86

3.3. Crystalline phases and chemical compositions of MKPCs immobilizing SCPWs

The XRD patterns of W0 and W50 after curing for 28 d showed peaks from both struvite-K and periclase (Fig. 4). W50 showed additional bands from quartz (SiO_2), K-feldspar ($KAlSi_3O_8$), plagioclase ($NaAlSi_3O_8$–$CaAl_2Si_2O_8$), and calcite ($CaCO_3$), all of which originated from the SCPWs (Fig. 4). Periclase (MgO) patterns were also present because MgO was added in excess of the stoichiometric molar ratio needed to form struvite-K. No other crystalline secondary reaction products were observed after the addition of SCPWs, although the formation of amorphous phases such as calcium phosphate cannot be ruled out. In addition, no new phases related to the addition of Cs, Co, and Sr were observed.

The scanning electron micrographs and compositional mapping of W50 revealed MgO, sands, cement paste particles, and struvite-K (Fig. 5). MgO originated mainly from the starting materials, which contained excess MgO over the stoichiometric composition of struvite-K. Cracks formed because the polished surface became dehydrated during vacuum drying and analysis [38]. Sand particles composed mostly of SiO_2 are the main ingredient of SCWPs, along with cement paste particles composed of CaO–SiO_2. No secondary reaction products were detected. Struvite-K crystals composed of Mg, K, and P formed homogeneously. Most of the sands and cement

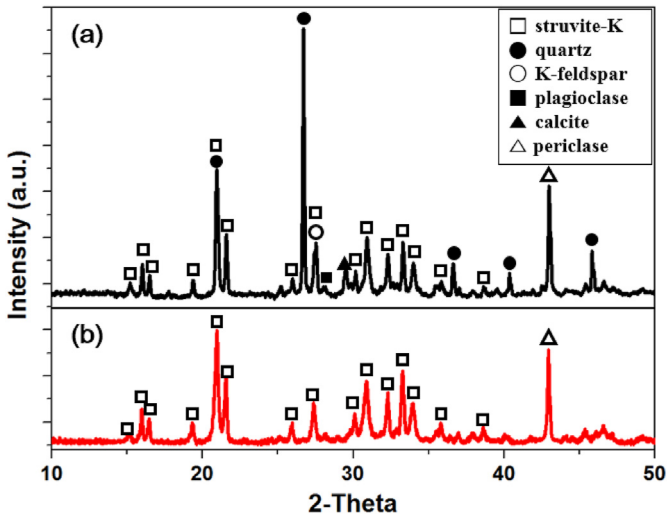

Fig. 4. X-ray diffraction patterns of magnesium potassium phosphate cement specimens with (a) 50 wt% and (b) 0 wt% simulated concrete powder wastes, after curing for 28 d.

particles from SCPWs and the unreacted MgO particles appear to be surrounded by the struvite-K phase.

3.4. Evaluation of waste acceptance criteria

3.4.1. Compressive strength of MKPCs after thermal cycling and water immersion

W50 MKPCs that had been cured for 28 d were evaluated (Table 6). The compressive strength of cementitious solids usually decreases after thermal cycling tests because the alternating freezing and thawing of the internal water impose stress [48]. Our specimens did not develop any visible cracks; however, an average weight decrease of 3% was observed after 30 thermal cycles. The compressive strength of the specimens after thermal cycling was 46.72 MPa, which is 17% less than that of the pristine specimens but still well above the WAC of 3.45 MPa.

Table 6
Compressive strength [MPa] of magnesium potassium phosphate cement specimens after thermal cycling and water immersion tests. Specimens contained 50 wt% simulated concrete powder wastes and were cured for 28 d.

Specimen No.	Condition		
	Pristine	Thermal cycling	Water immersion
1	61.39	40.52	51.58
2	51.73	50.55	44.35
3	55.70	49.09	51.21
Average ± s.d.	56.27 ± 4.86	46.72 ± 5.42	49.05 ± 4.07

After immersion in water for 90 d, no visible external deterioration was observed. However, the weight decreased by 5%, and the compressive strength decreased by 13% to 49.05 MPa, which is still higher than 3.45 MPa. The observed weight loss during immersion is mainly due to the washing out of residual unreacted binder and leaching of the MKPC components [49]. Our results demonstrate that these MKPC specimens, that bore 50 wt% SCPWs and were cured for 28 d, satisfied the WACs for thermal cycling and water immersion.

3.4.2. Leachability index

The leachability indices (LIs) of three representative radionuclides (Cs, Co, Sr) in contaminated concrete were evaluated using the ANS 16.1 method (Table 7). The LIs of Cs, Co, and Sr were 11.45, 17.63, and 15.66, respectively, satisfying the WAC of >6. When radioactive CsCl solidifies inside MKPCs, Cs^{+} is immobilized in the form of $MgCs_xK_{1-x}PO_4.6H_2O$, which has $11.5 \leq LI \leq 11.7$ [50].

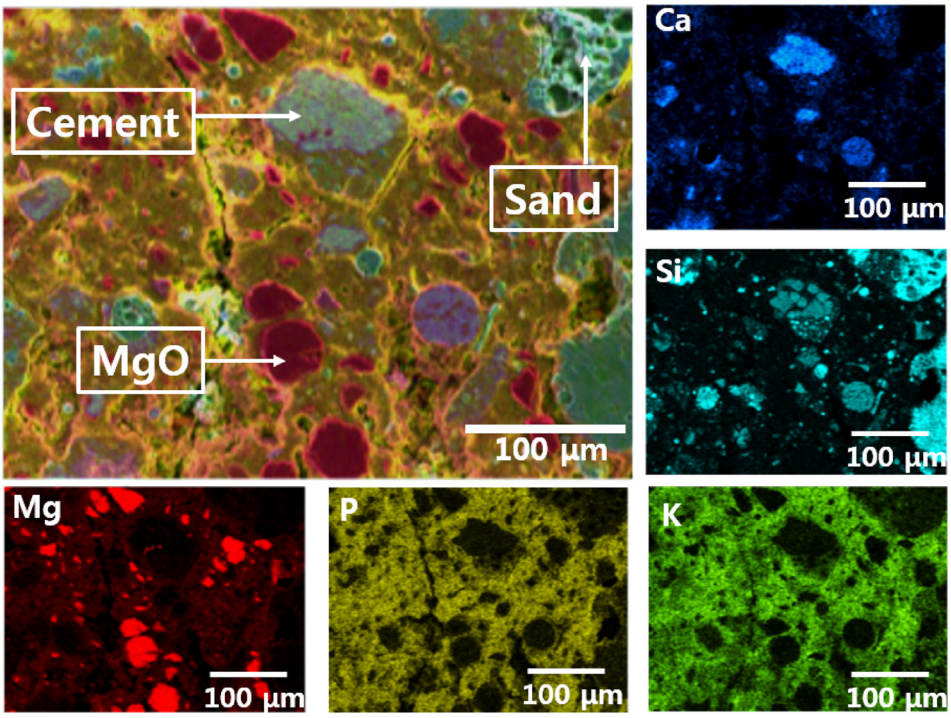

Fig. 5. Scanning electron micrograph of magnesium potassium phosphate cements with 50 wt% simulated concrete powder wastes and compositional mapping of Ca, Si, Mg, P, and K.

Table 7
Diffusivity (D) [cm^2/s] and leachability indices (LI) of Cs, Co, and Sr evaluated using the ANS 16.1 method.

Sample day	Element					
	Cs		Co		Sr	
	D	LI	D	LI	D	LI
0.083	1.62×10^{-13}	12.79	8.92×10^{-18}	17.05	7.37×10^{-17}	16.13
0.292	1.35×10^{-11}	10.87	1.65×10^{-16}	15.78	8.54×10^{-16}	15.07
1	9.97×10^{-12}	11.00	6.63×10^{-17}	16.18	6.59×10^{-16}	15.18
2	1.75×10^{-11}	10.76	3.13×10^{-17}	16.50	3.83×10^{-16}	15.42
3	1.48×10^{-11}	10.83	1.41×10^{-17}	16.85	7.54×10^{-16}	15.12
4	9.39×10^{-12}	11.03	4.15×10^{-18}	17.38	8.88×10^{-15}	14.05
5	1.73×10^{-13}	12.76	1.37×10^{-18}	17.86	1.44×10^{-15}	14.84
19	4.17×10^{-12}	11.38	9.67×10^{-20}	19.01	3.11×10^{-18}	17.51
47	3.15×10^{-12}	11.50	2.36×10^{-20}	19.63	1.86×10^{-17}	16.73
90	2.38×10^{-12}	11.62	9.97×10^{-21}	20.00	2.80×10^{-17}	16.55
Average LI		11.45		17.63		15.66

Previous use of MPKCs to immobilize alkaline supernatant liquid wastes from Hanford (USA) and Mayak (Russia) showed $11.4 \leq LI \leq 11.5$ for Cs and $10.9 \leq LI \leq 13.2$ for Sr, respectively [51]. The MKPC waste forms developed in the current study exhibit LIs comparable to those reported previously. Furthermore, the addition of SCPWs did not degrade the resistance of MKPCs to leaching. The MKPCs achieved high enough resistance to elemental leaching to be used for immobilization of the radioactive concrete powder wastes that are generated during decommissioning of nuclear facilities.

4. Conclusions

To determine the efficacy of magnesium potassium phosphate cements (MKPCs) for immobilizing radioactive concrete wastes, MKPCs were mixed with up to 50 wt% of simulated concrete powder wastes (SCPWs). Struvite-K phases formed in the waste forms and surrounded the SCPW sand and cement particles. The compressive strength of MKPC specimens increased from 41 to 56 MPa with the addition of 50 wt% SCPWs. The MKPC specimens that contained 50 wt% SCPWs were subjected to thermal-cycling and water-immersion tests. After the tests, the compressive strength of the specimens remained >45 MPa, which satisfies the waste acceptance criterion. The leaching indices of Cs, Co, and Sr, analyzed following the ANS 16.1 procedure, were 11.45, 17.63, and 15.66, respectively; these also satisfy the waste acceptance criterion. Our findings demonstrate that MKPCs can be used to immobilize radioactive concrete wastes generated during the decommissioning of nuclear power plants.

Declaration of Competing Interest

The authors declare that they have no known competing financial interests or personal relationships that could have appeared to influence the work reported in this paper.

Acknowledgments

This work was supported by the National Research Foundation of Korea (NRF) grant funded by the Korean government (Ministry of Science and ICT) (No. 2017M2B2B1072405).

References

[1] IAEA, Nuclear Power Reactors in the World, 2019. Vienna, https://www.iaea.org/publications/13552/nuclear-power-reactors-in-the-worlddf.
[2] A. Crégut, J. Roger, Inventory of information for the identification of guiding principles in the decommissioning of nuclear installations, Euratom. No. EUR-13 (1991) 90.
[3] IAEA, Radiological Characterization of Shut Down Nuclear Reactors for Decommissioning Purposes, 1998. Vienna, http://www-pub.iaea.org/MTCD/Publications/PDF/TRS389_scr.pdf.
[4] M. Kinno, K.I. Kimura, T. Nakamura, Raw materials for low-activation concrete neutron shields, J. Nucl. Sci. Technol. 39 (2002) 1275–1280, https://doi.org/10.1080/18811248.2002.9715321.
[5] K.S. Dickerson, M.J. Wilson-Nichols, M.I. Morris, Contaminated Concrete: Occurrence and Emerging Technologies for DOE Decontamination, Oak Ridge National Lab., 1995. No. DOE/ORO–2034.
[6] M.J. Angus, S.R. Hunter, J. Ketchen, Classification of contaminated and neutron-activated concretes from nuclear facilities prior to their decontamination or decommissioning, Waste Manag. 90 (1990). CONF-900210–VOL.2.
[7] NEA, The NEA Co-operative Programe on Decommissioning, Decontamination and Demolition of Concrete Structures, 2011.
[8] M. Hashish, D.C. Echert, Abrasive-waterjet deep kerfing and waterjet surface cleaning for nuclear facilities, J. Eng. Ind. 111 (1989) 269–281, https://doi.org/10.1115/1.3188759.
[9] M. Castellote, C. Andrade, C. Alonso, Nondestructive decontamination of mortar and concrete by electro-kinetic methods: application to the extraction of radioactive heavy metals, Environ. Sci. Technol. 36 (2002) 2256–2261, https://doi.org/10.1021/es015683c.
[10] D. Gurau, R. Deju, The use of chemical gel for decontamination during decommissioning of nuclear facilities, Radiat. Phys. Chem. 106 (2015) 371–375, https://doi.org/10.1016/j.radphyschem.2014.08.022.
[11] A.N. Nikolaev, O.K. Karlina, A.Y. Yurchenko, Y.V. Karlin, Assessment of 137Cs decontamination of concrete by the reagent method, At. Energy. 112 (2012) 57–62, https://doi.org/10.1007/s10512-012-9524-7.
[12] P.V. Samuleev, W.S. Andrews, K.A.M. Creber, P. Azmi, D. Velicogna, W. Kuang, K. Volchek, Decontamination of radionuclides on construction materials, J. Radioanal. Nucl. Chem. 296 (2013) 811–815, https://doi.org/10.1007/s10967-012-2146-7.
[13] B.Y. Min, W.K. Choi, K.W. Lee, Separation of clean aggregates from contaminated concrete waste by thermal and mechanical treatment, Ann. Nucl. Energy 37 (2010) 16–21, https://doi.org/10.1016/j.anucene.2009.10.010.
[14] A.S. Wagh, Chemically Bonded Phosphate Ceramics: Twenty-First Century Materials with Diverse Applications, second ed., 2016, https://doi.org/10.1016/B978-0-08-044505-2.X5000-5. Amsterdam.
[15] B.E.I. Abdelrazig, J.H. Sharp, B. El-Jazairi, The microstructure and mechanical properties of mortars made from magnesia-phosphate cement, Cement Concr. Res. 19 (1989) 247–258, https://doi.org/10.1016/0008-8846(89)90089-6.
[16] E. Soudée, J. Péra, Influence of magnesia surface on the setting time of magnesia-phosphate cement, Cement Concr. Res. 32 (2002) 153–157, https://doi.org/10.1016/S0008-8846(01)00647-0.
[17] Q. Yang, B. Zhu, X. Wu, Characteristics and durability test of magnesium phosphate cement-based material for rapid repair of concrete, Mater. Struct. 33 (2000) 229–234, https://doi.org/10.1007/bf02479332.
[18] F. Qiao, C.K. Chau, Z. Li, Property evaluation of magnesium phosphate cement mortar as patch repair material, Construct. Build. Mater. 24 (2010) 695–700, https://doi.org/10.1016/j.conbuildmat.2009.10.039.
[19] D. Singh, V.R. Mandalika, S.J. Parulekar, A.S. Wagh, Magnesium potassium phosphate ceramic for 99Tc immobilization, J. Nucl. Mater. 348 (2006) 272–282, https://doi.org/10.1016/j.jnucmat.2005.09.026.
[20] I. Buj, J. Torras, M. Rovira, J. de Pablo, Leaching behaviour of magnesium phosphate cements containing high quantities of heavy metals, J. Hazard Mater. 175 (2010) 789–794, https://doi.org/10.1016/j.jhazmat.2009.10.077.
[21] A.S. Wagh, R. Strain, S.Y. Jeong, D. Reed, T. Krause, D. Singh, Stabilization of Rocky Flats Pu-contaminated ash within chemically bonded phosphate ceramics, J. Nucl. Mater. 265 (1999) 295–307, https://doi.org/10.1016/S0022-3115(98)00650-3.
[22] D. Chartier, J. Sanchez-Canet, P. Antonucci, S. Esnouf, J.P. Renault, O. Farcy, D. Lambertin, S. Parraud, H. Lamotte, C.C.D. Coumes, Behaviour of magnesium phosphate cement-based materials under gamma and alpha irradiation, J. Nucl. Mater. (2020), https://doi.org/10.1016/j.jnucmat.2020.152411.
[23] S.E. Vinokurov, S.A. Kulikova, V.V. Krupskaya, B.F. Myasoedov, Magnesium Potassium Phosphate Compound for Radioactive Waste Immobilization: Phase Composition, Structure, and Physicochemical and Hydrolytic Durability, Radiochemistry, 2018, https://doi.org/10.1134/S1066362218010125.
[24] D.A. Burbank, Waste Acceptance Criteria for the Immobilized Low Activity Waste (ILAW) Disposal Facility, 2002, https://doi.org/10.2172/807982. United States.
[25] J.J. Kim, D.J. Kim, S.T. Kang, J.H. Lee, Influence of sand to coarse aggregate ratio on the interfacial bond strength of steel fibers in concrete for nuclear power plant, Nucl. Eng. Des. 252 (2012) 1–10, https://doi.org/10.1016/j.nucengdes.2012.07.004.
[26] L.J. Gardner, S.A. Bernal, S.A. Walling, C.L. Corkhill, J.L. Provis, N.C. Hyatt, Response to the discussion by Hongyan Ma and Ying Li of the paper "Characterization of magnesium potassium phosphate cement blended with fly ash and ground granulated blast furnace slag, Cement Concr. Res. 103 (2018) 249–253, https://doi.org/10.1016/j.cemconres.2017.07.011.
[27] G.B. Josephson, J.H. Westsik, R.P. Pires, J. Bickford, M.W. Foote, Engineering-scale Demonstration of DuraLith and Ceramicrete Waste Forms, Pacific Northwest National Lab.(PNNL), 2011, https://doi.org/10.2172/1027183. Richland, WA (United States).

[28] M. Le Rouzic, T. Chaussadent, L. Stefan, M. Saillio, On the influence of Mg/P ratio on the properties and durability of magnesium potassium phosphate cement pastes, Cement Concr. Res. 96 (2017) 27–41, https://doi.org/10.1016/j.cemconres.2017.02.033.
[29] H. Ma, B. Xu, Z. Li, Magnesium potassium phosphate cement paste: degree of reaction, porosity and pore structure, Cement Concr. Res. 65 (2014) 96–104, https://doi.org/10.1016/j.cemconres.2014.07.012.
[30] H. Ma, Y. Li, Discussion of the paper "Characterisation of magnesium potassium phosphate cement blended with fly ash and ground granulated blast furnace slag" by L.J. Gardner et al, Cement Concr. Res. 103 (2018) 245–248, https://doi.org/10.1016/j.cemconres.2017.07.013.
[31] ASTM, Test Method for Thermal Cycling of Electroplated Plastics, 1985.
[32] ANS, Measurement of the Leachability of Solidified Low-Level Radioactive Wastes by a Short-Term Procedure, 2009.
[33] M.J. Varas, M.A. De Buergo, R. Fort, Natural cement as the precursor of Portland cement: methodology for its identification, Cement Concr. Res. 35 (2005) 2055–2065, https://doi.org/10.1016/j.cemconres.2004.10.045.
[34] P. Hou, R. Zhang, X. Cheng, Case study of the gradient features of in situ concrete, Case Stud. Constr. Mater. 1 (2014) 154–163, https://doi.org/10.1016/j.cscm.2014.08.003.
[35] K. De Weerdt, M. Ben Haha, G. Le Saout, K.O. Kjellsen, H. Justnes, B. Lothenbach, Hydration mechanisms of ternary Portland cements containing limestone powder and fly ash, Cement Concr. Res. 41 (2011) 279–291, https://doi.org/10.1016/j.cemconres.2010.11.014.
[36] L. Alarcon-Ruiz, G. Platret, E. Massieu, A. Ehrlacher, The use of thermal analysis in assessing the effect of temperature on a cement paste, Cement Concr. Res. 35 (2005) 609–613, https://doi.org/10.1016/j.cemconres.2004.06.015.
[37] P. Chindaprasirt, C. Jaturapitakkul, T. Sinsiri, Effect of fly ash fineness on microstructure of blended cement paste, Construct. Build. Mater. 21 (2007) 1534–1541, https://doi.org/10.1016/j.conbuildmat.2005.12.024.
[38] L.J. Gardner, S.A. Bernal, S.A. Walling, C.L. Corkhill, J.L. Provis, N.C. Hyatt, Characterisation of magnesium potassium phosphate cements blended with fly ash and ground granulated blast furnace slag, Cement Concr. Res. 74 (2015) 78–87, https://doi.org/10.1016/j.cemconres.2015.01.015.
[39] W. Zhu, J.J. Hughes, N. Bicanic, C.J. Pearce, Nanoindentation mapping of mechanical properties of cement paste and natural rocks, Mater. Char. 58 (2007) 1189–1198, https://doi.org/10.1016/j.matchar.2007.05.018.
[40] H. Ma, B. Xu, J. Liu, H. Pei, Z. Li, Effects of water content, magnesia-to-phosphate molar ratio and age on pore structure, strength and permeability of magnesium potassium phosphate cement paste, Mater. Des. 64 (2014) 497–502, https://doi.org/10.1016/j.matdes.2014.07.073.
[41] I. Buj, J. Torras, D. Casellas, M. Rovira, J. de Pablo, Effect of heavy metals and water content on the strength of magnesium phosphate cements, J. Hazard Mater. 170 (2009) 345–350, https://doi.org/10.1016/j.jhazmat.2009.04.091.
[42] A.J. Wang, J. Zhang, J.M. Li, A.B. Ma, L.T. Liu, Effect of liquid-to-solid ratios on the properties of magnesium phosphate chemically bonded ceramics, Mater. Sci. Eng. C 33 (2013) 2508–2512, https://doi.org/10.1016/j.msec.2013.02.014.
[43] S. Diamond, A critical comparison of mercury porosimetry and capillary condensation pore size distributions of portland cement pastes, Cement Concr. Res. (1971), https://doi.org/10.1016/0008-8846(71)90058-5.
[44] H. Dong, P. Gao, G. Ye, Characterization and comparison of capillary pore structures of digital cement pastes, Mater. Struct. Constr. (2017), https://doi.org/10.1617/s11527-017-1023-9.
[45] R. Kumar, B. Bhattacharjee, Porosity, pore size distribution and in situ strength of concrete, Cement Concr. Res. (2003), https://doi.org/10.1016/S0008-8846(02)00942-0.
[46] H. Ma, B. Xu, Potential to design magnesium potassium phosphate cement paste based on an optimal magnesia-to-phosphate ratio, Mater. Des. 118 (2017) 81–88, https://doi.org/10.1016/j.matdes.2017.01.012.
[47] D.P. Bentz, Influence of water-to-cement ratio on hydration kinetics: simple models based on spatial considerations, Cement Concr. Res. (2006), https://doi.org/10.1016/j.cemconres.2005.04.014.
[48] S. V Mattigod, J.H. Westsik, C.-W. Chung, M.J. Lindberg, K.E. Parker, Waste Acceptance Testing of Secondary Waste Forms: Cast Stone, Ceramicrete and DuraLith, Pacific Northwest National Lab.(PNNL), 2011, https://doi.org/10.2172/1027185. Richland, WA (United States).
[49] D. Singh, R. Ganga, J. Gaviria, Y. Yusufoglu, Secondary Waste Form Testing : Ceramicrete Phosphate Bonded ceramics., ANL-11/16, Argonne Natl. Labratory, 2011, https://doi.org/10.2172/1020703.
[50] A.S. Wagh, S.Y. Sayenko, V.A. Shkuropatenko, R.V. Tarasov, M.P. Dykiy, Y.O. Svitlychniy, V.D. Virych, Y.A. Ulybkina, Experimental study on cesium immobilization in struvite structures, J. Hazard Mater. 302 (2016) 241–249, https://doi.org/10.1016/j.jhazmat.2015.09.049.
[51] S.E. Vinokurov, Y.M. Kulyako, O.M. Slyuntchev, S.I. Rovny, B.F. Myasoedov, Low-temperature immobilization of actinides and other components of high-level waste in magnesium potassium phosphate matrices, J. Nucl. Mater. 385 (2009) 189–192, https://doi.org/10.1016/j.jnucmat.2008.09.053.